





METHODS AND APPROACHES

Excitation–Contraction Coupling

A novel method for determining murine skeletal muscle fiber type using autofluorescence lifetimes

Carlo Manno¹, Eshwar Tammineni¹, Lourdes Figueroa¹, Yuriana Oropeza-Almazán¹, and Eduardo Rios¹

This work describes a simple way to identify fiber types in living muscles by fluorescence lifetime imaging microscopy (FLIM). We quantified the mean values of lifetimes τ_1 and τ_2 derived from a two-exponential fit in freshly dissected mouse flexor digitorum brevis (FDB) and soleus muscles. While τ_1 values changed following a bimodal behavior between muscles, the distribution of τ_2 is shifted to higher values in FDB. To understand the origin of this difference, we obtained maps of autofluorescence lifetimes of flavin mononucleotide and dinucleotide (FMN/FAD) in cryosections, where excitation was set at 440 nm and emission at a bandwidth of between 500 and 570 nm, and paired them with immunofluorescence images of myosin heavy chain isoforms, which allowed identification of fiber types. In soleus, τ_2 was 3.16 ns for type I (SD 0.11, 97 fibers), 3.45 ns for IIA (0.10, 69), and 3.46 ns for IIX (0.12, 65). In FDB muscle, τ_2 was 3.17 ns for type I (0.08, 22), 3.46 ns for IIA (0.16, 48), and 3.66 ns for IIX (0.15, 43). From τ_2 distributions, it follows that an FDB fiber with $\tau_2 > 3.3$ ns is expected to be of type II, and of type I otherwise. This simple classification method has first and second kind errors estimated at 0.02 and 0.10, which can be lowered by reducing the threshold for identification of type I and increasing it for type II. Lifetime maps of autofluorescence, therefore, constitute a tool to identify fiber types that, for being practical, fast, and noninvasive, can be applied in living tissue without compromising other experimental interventions.

Introduction

Mammalian skeletal muscles are composed of heterogeneous bundles of myofibers, classified into fiber types according to their particular myosin heavy chain (MHC) isoform and metabolic activity. Slow-twitch-type I-fibers are classified as oxidative, and fast-twitch-type II-fibers as a mixture of oxidative (IIA) and glycolytic (IIB and IIX; [Schiaffino et al., 1989](#)). Each of these fiber types is characterized by differences in excitation–contraction coupling (ECC) properties, such as the voltage dependence of intramembrane movement of ECC voltage sensors (“charge movement”; [Hollingworth and Marshall, 1981](#)), and content of the proteins that control the kinetics of calcium transients ([Baylor and Hollingworth, 2003](#); [Calderon-Velez et al., 2010](#)). The sum of these characteristics provides a specialization to each fiber type in managing intracellular calcium, with consequent divergence in their calcium signals.

In addition to the above-mentioned functional properties, the signature metabolic characteristics of oxidative and glycolytic fiber types include their mitochondrial morphology, role, and

content of metabolites ([Johnson et al., 2007](#)). In this sense, essential metabolites, the flavoprotein prosthetic group flavin adenine mononucleotide and dinucleotide (FMNH₂ and FADH₂), which serve important functions as metabolic electron carriers in mitochondrial bioenergetics and subsequent ATP production, can be used as an endogenous monitor of cellular metabolism. To this end, metabolic imaging is based on the fact that the oxidized forms of flavin adenine mono- and dinucleotide—FMN/FAD—are inherently fluorescent, and have been extensively used as markers to identify the metabolic activity of several cells including skeletal muscle fibers (for review, see [Kolenc and Quinn, 2019](#)). A drawback of fluorescence intensity-based FMN/FAD measurements is that these intrinsic fluorophores have a quantum yield an order of magnitude lower than commonly used monitors. Therefore, tracking variations of metabolic state via imaging finds inconsistencies, because values depend on parameters used to collect data, including excitation light intensity, light scattering, and photobleaching ([Periasamy and Clegg, 2009](#), and examples in the Supplemental material).

¹Department of Physiology and Biophysics, Rush University, Chicago, IL.

Correspondence to Carlo Manno: carlos_manno@rush.edu

This work is part of a special issue on excitation–contraction coupling.

© 2022 Manno et al. This article is distributed under the terms of an Attribution–Noncommercial–Share Alike–No Mirror Sites license for the first six months after the publication date (see <http://www.rupress.org/terms/>). After six months it is available under a Creative Commons License (Attribution–Noncommercial–Share Alike 4.0 International license, as described at <https://creativecommons.org/licenses/by-nc-sa/4.0/>).

In this work, to noninvasively identify fiber types in living muscles, we employ fluorescence lifetime imaging microscopy (FLIM) of the fibers' autofluorescence; the approach overcomes the limitations of fluorescence intensity-based measurement because it can extract metabolic information independently of fluorophore concentration, acquisition region area, and a variety of differences in the molecular microenvironment, such as pH, temperature, and viscosity (Lakowicz, 2006; Chen et al., 2014).

The fluorescence decay curve of FAD and related flavins (including riboflavin and flavin mononucleotide, FMN) consists of two exponential components of different lifetime. These lifetime fluorescence components resemble the emission by the principal electron donor, reduced NADH, where the short lifetime (τ_1) is ascribed to free and the long lifetime (τ_2) is characteristic of NADH bound to a protein (Lakowicz et al., 1992; Blinova et al., 2005). In this particular case, τ_1 is attributed to free FAD/FMN, and the long lifetime (τ_2) is characteristic of FAD bound to a flavoprotein—largely lipoamide dehydrogenase.

In the present study, the distribution of the two lifetimes was quantified in longitudinal and transverse sections of freshly dissected FDB and soleus murine muscles. It was found that, while the distribution of τ_1 changes only slightly, that of τ_2 differs sharply between fast and slow muscles. Hypothesizing that the diverging lifetimes reflect different fiber-type composition, maps of autofluorescence lifetimes were obtained in cryosections of each of these muscles ("Maps" refer to 2-D pixel-by-pixel representations of the autofluorescence, where the color-coded value at each pixel is that of a lifetime parameter, rather than the usual intensity). Individually paired lifetime maps and immunofluorescence images of MHC isoforms revealed striking lifetime differences between fiber types. This comparison led to a simple method to identify fiber types via a rapid, noninvasive, label-free imaging procedure, which should help standardize functional assays for which results are expected to depend on fiber type.

Materials and methods

Ethical approval

Protocols on usage, care, transfection, and killing of animals were approved by the Institutional Animal Care and Use Committee of Rush University, and were consistent with their ethical standards, and in compliance with the guidelines of the Animal Care and Welfare Act.

Animals

6–12-wk-old WT mice of the strain C57BL/6 were obtained from Charles River Breeding Laboratories, Wilmington, MA. Animals were euthanized by CO₂ inhalation and subsequent cervical dislocation. FDB and soleus muscles were immediately removed and either prepared for cryosectioning or immobilized in a custom 3-D-printed chamber (Manno et al., 2017) for FLIM measurements and imaging.

Solutions

PBS (in mM): 137 NaCl, 2.7 KCl, 10 Na₂HPO₄, and 1.8 KH₂PO₄. Relaxing solution (in mM): 145 K-glutamate, 10 HEPES, 1 MgCl₂,

0.1 EGTA. pH was adjusted to 7.4 and osmolarity to 310 mOsm/liter. A 120-mM stock of flavin adenine dinucleotide (F6625; Sigma-Aldrich) was prepared in relaxing solution. Dilutions of FAD were prepared at the following concentrations (in mM): 0.01, 0.1, 0.5, 1, 12, 20, and 50, using relaxing solution.

FLIM of autofluorescence

The basic technique applied here is the FLIM imaging of autofluorescence in different fiber types, in vivo, in fixed muscles, and in solutions containing FAD. The mode of lifetime imaging used was time-correlated single photon counting, implemented in a laser-scanning confocal imaging system (Falcon SP8; Leica Microsystems) with continuously adjustable excitation wavelength and high-sensitivity "HyD" hybrid detectors. The technique, which records single photons with picosecond resolution (Fig. 1), works as a stopwatch that stores the time elapsed between the excitation pulse (A) and the recording of the emitted photon (D, called "arrival time" or "lifetime," a term we prefer for brevity). The excitation pulses (the 40-MHz output from a pulsed diode laser [PDL 800-D; PicoQuant]) provide a 25-ns window between them for recording multiple photons and their arrival times. A first stage in FLIM is the acquisition of "lifetime images," in our case arrays of 256 × 256 pixels, where the values are pixel averages of all photon arrival times recorded there (example in Fig. 2, A a and c). The acquisition is carried out in scans, consisting in one excitation pulse per pixel and collection of the emitted photons during the 25-ns window between pulses. One lifetime image is usually built from 20 scans, yielding an average of 300 photons/pixel inside most parts of the imaged area. The objectives used to acquire large image fields and individual fiber measurements were, respectively, HC PL Fluotar 20×/0.55 dry and HC PL APO CS2 63×/1.2 water (Leica).

Lifetime images (and the associated "phasor plot" [Fig. 1E], described in the Appendix) provide a first view of the distribution of photon arrival times. On the basis of these images, further analysis consists in accumulating lifetimes from a region of interest (ROI), rectangular in intact muscles, or circular in muscle cross-sections, using a similar area of acquisition between fibers (Fig. 1, B a and C a). Collected lifetimes in individual pixels or in ROIs are plotted as histograms $I(t)$ (where I represents photon count per unit time interval at arrival time t), also known as fluorescence decay or fluorescence response curves (Fig. 1E). These curves were parametrized by fitting with the sum of multiple exponentials. The two-exponential model was considered adequate for fitting the data (which was true in most cases) when it yielded χ^2 values <1.5:

$$I(t) = A_1 \cdot e^{-t/\tau_1} + A_2 \cdot e^{-t/\tau_2}. \quad (1)$$

Determination of myofiber type by immunofluorescence

Fiber types were identified by immunofluorescence imaging analysis using monoclonal antibodies specific to MHC isoforms characteristic of each cell type.

FDB and soleus cross-sections were prepared as described by Beedle (2016). Muscles were dissected and introduced into the Optimal Cutting Temperature compound (Thermo Fisher

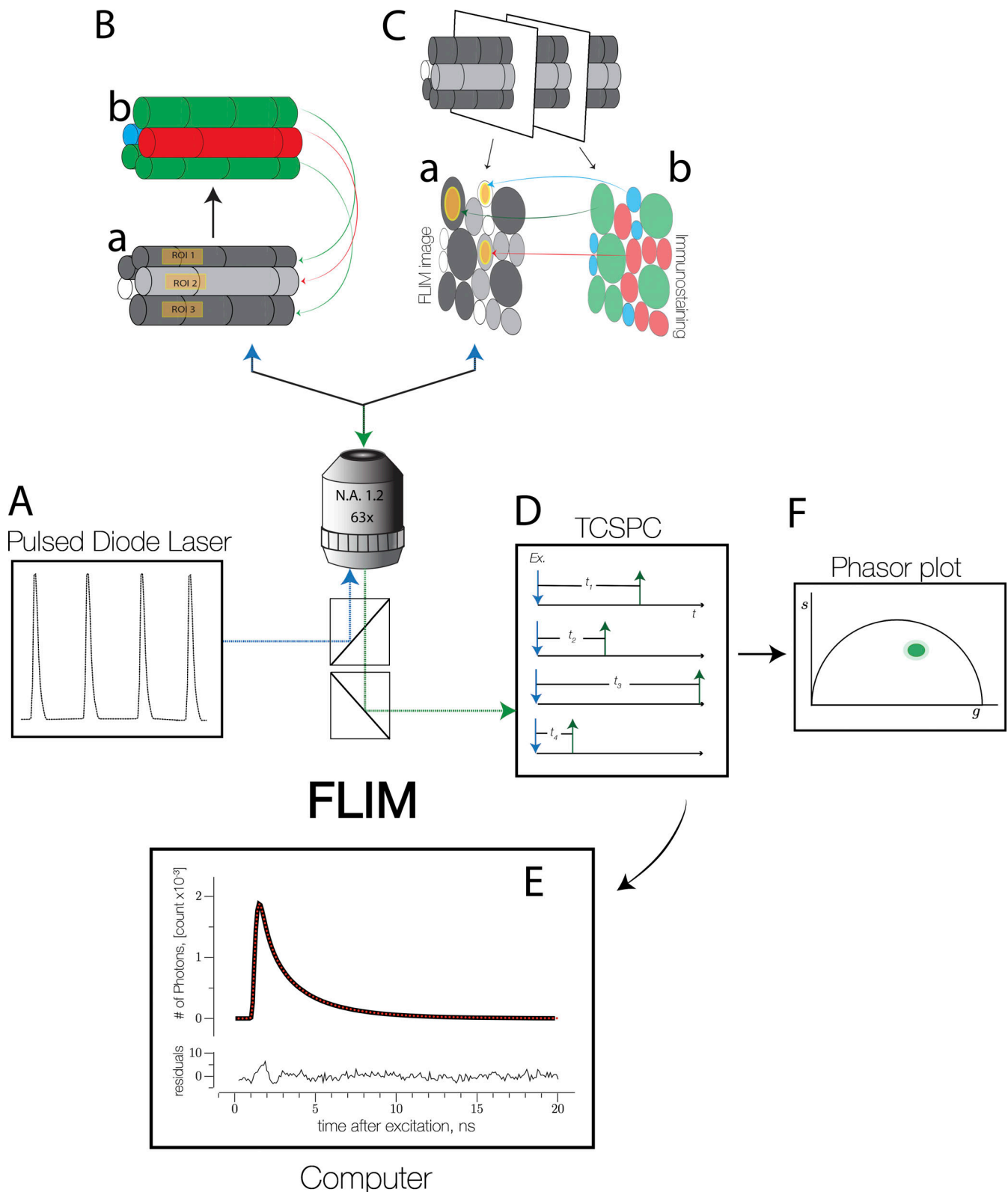
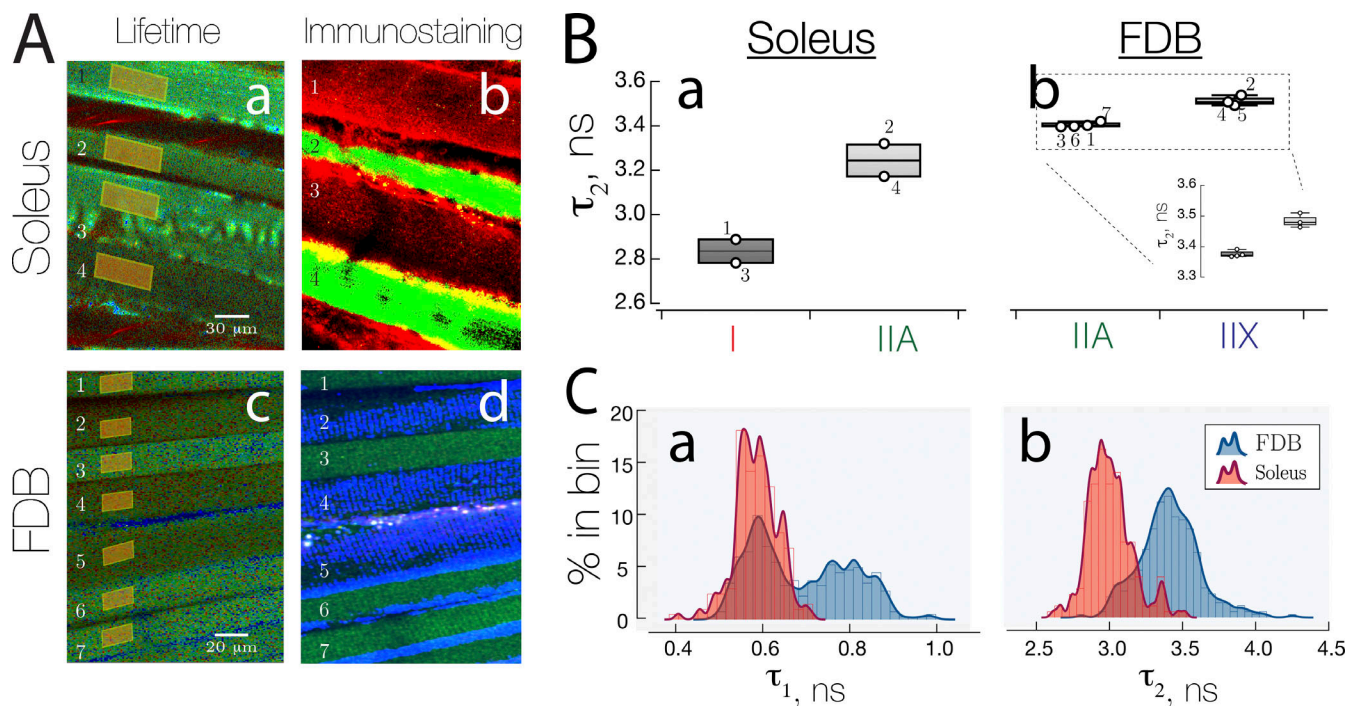


Figure 1. **Methods of fluorescence lifetime imaging microscopy.** (A) Laser pulses (Ex/Em 440/500–570 nm) were focused over the unstained tissue. (B and C) FLIM and immunostaining imaging performed sequentially in fresh whole muscle or in muscle cross-sections. Acquisition of autofluorescence lifetimes is done first, with fits of $I(t)$ in regions marked in yellow (B a and C a), followed by immunostaining (B b and C b), so that fit parameters and immunologic typing can be put in correspondence. (D) Representation of time-domain FLIM; arrival times (t_i) are quantified using a time-correlated single photon counting (TCSPC) unit, by sequentially exciting a solution or tissue, and recording the time it takes for the emission of each fluorescence photon. (E) Histogram $I(t)$ of arrival times, defined at individual spatial location (pixels or multipixel regions). A multiexponential fit provides the unique parameters (A_i , τ_i). An additional outcome is the number of photon counts or total emission (Te). The lower plot is the residual of a two-exponential fit. (F) Graphic implementation of the method based on the phasor transformation.



Scientific), and subsequently transferred into isopentane, previously cooled in liquid nitrogen for 10 min. Cryopreserved samples were cut with a Cryostat CM1850 (Leica) as 10 μm -thick sections transverse to the fiber axis. Frozen cross-sections were fixed in 4% PFA for 20 min and washed in PBS. Fixed cross-sections were incubated in 0.2% Triton X-100 (Sigma-Aldrich) for 30 min, and then incubated in 5% goat serum (G9023; Sigma-Aldrich) for 1 h. Incubation in primary antibodies was done overnight at 4°C. Cross-sections were incubated in secondary antibodies for 2 h at room temperature.

Preparation of whole muscle fibers for immunostaining: muscles were fixed in 4% PFA for 25 min and washed with PBS. Fixed muscles were kept in a glass chamber with acetone (Millipore Sigma) for 20 min at -20°C . Permeabilized muscles were incubated in 2% Triton X-100 for 30 min, then in 5% goat serum (G9023; Sigma-Aldrich) for 1 h.

Preparation of whole muscle fibers for immunostaining: muscles were fixed in 4% PFA for 25 min and washed with PBS. Fixed muscles were kept in a glass chamber with acetone (Millipore Sigma) for 20 min at -20°C . Permeabilized muscles were incubated in 2% Triton X-100 for 30 min, then in 5% goat serum (G9023; Sigma-Aldrich) for 1 h.

Incubation with primary antibody was overnight at 4°C and secondary antibodies for 2 h at room temperature.

Primary antibodies were applied at 20 $\mu\text{g}/\text{ml}$ for cross-sections and at 60 $\mu\text{g}/\text{ml}$ for whole muscles as follows: type I, BA-F8; type IIA, SC-71; and type IIX, 6H1 (all from Developmental Studies Hybridoma Bank). Secondary antibodies (10 $\mu\text{g}/\text{ml}$): type I, A-21242; type IIA, A-21121; and type IIX, A-21044

(all from Thermo Fisher Scientific). Signals were acquired in sequential mode, which eliminates crosstalk between emissions at different wavelengths.

For the identification of fiber type in intact muscle preparations we used an application module supplied by Leica, which provides an overview of large fields in immunostained whole muscle bundles.

Statistics and presentation of replicates

The measurements compared in the present study are typically quantitative features of N individuals (mice) with n_i replications (myofibers) for individual mouse i . The total number of replications (myofibers, images, cases) used in a study is denoted as $m = \sum n_i$. Statistical significance of the difference between variables was determined using hierarchical, a.k.a. nested analysis (Sikkel et al., 2017; Lazic et al., 2018). Means are calculated conventionally, averaging over all measurements, for example:

$$\bar{\tau} = \frac{\sum_{i=1}^N n_i \sum_{j=1}^{n_i} \tau_{ij}}{\sum_{i=1}^N n_i}. \quad (2)$$

Then, for evaluation of statistical significance of differences, an effective number of cases is calculated, which corrects for the grouping or clustering of replicates from the same individual, thus avoiding pseudoreplication (Lazic et al., 2018). The hierarchical analysis was carried out in the programming environment R, using RStudio (<https://www.rstudio.com/about/>).

The illustration of comparisons between measured variables is done with box plots, which show median (solid lines), bounds

of box (75th to 25th percentiles), and whiskers representing 95% in the data set.

Online supplemental material

Demonstration that intensity of autofluorescence could be useful for myofiber typing but has significant disadvantages compared with the evaluation of fluorescence lifetimes. Fig. S1 shows identification of fiber types with immunostaining and FLIM images in soleus muscle cross-sections. Fig. S2 shows FLIM parameters measured in xt-linescan mode. Supplemental text provides parameters used to collect data, including excitation light intensity, light scattering, and photobleaching.

Results

Correspondence between fiber type and fluorescence lifetime

Fluorescence lifetimes in intact myofibers

Fluorescence lifetime measurements were carried out on intact fibers of freshly removed FDB and soleus muscles, stretched to the bottom of a glass chamber, so they could be visualized under the microscope. Fig. 2A a and c exemplify lifetime images (pixel-by-pixel maps of photon arrival times after pulse excitation [lifetimes], acquired as described in Materials and methods). The histograms $I(t)$ of lifetimes accumulated in ROIs drawn in every fiber (a.k.a. fluorescence decay curves) were fitted with Eq. 1. Such analysis of FLIM data provides several quantitative outcomes, including the four best-fit parameters (A_1 , A_2 , τ_1 , and τ_2 , as shown in Fig. 1E) and the total number of photons emitted (herein “total emission,” T_e). While all of them varied with fiber type, the change in τ_2 was most notable.

After lifetime imaging, muscles were fixed and immunostained for identification of MHC isoforms. Images in Fig. 2A b and d show immunofluorescence in the area with FLIM measurements. Based on the immunostaining, soleus muscles have a higher proportion of oxidative fibers of type I and IIA (red and green, respectively); and FDB of type IIA and glycolytic IIX (green and blue, respectively). τ_2 values for ROIs in every individual fiber in the images were grouped according to fiber type and their distribution represented with box plots (Fig. 2B). The distributions of τ_1 and τ_2 in multiple images of FDB and soleus, regardless of fiber type, are represented as histograms in Fig. 2C a and b, respectively. These histograms show that lower lifetimes, and consequently lower values of τ_1 and τ_2 are more frequently observed in soleus compared to FDB. τ_1 values are distributed with two different modes in FDB muscles—a confounding factor for any use of the difference in lifetimes. This was not the case for the distribution of τ_2 ; therefore, this was the parameter considered for further comparisons.

Fluorescence lifetimes in muscle cross-sections

To further evaluate the differences in lifetime distributions between fiber types, fibers in larger numbers were assessed by immunostaining of muscle cross-sections (Fig. 3). In the immunostained sections, fibers were numbered and colorized according to type (Fig. 3A b and d). Histograms of lifetimes $I(t)$, derived from ROIs covering most of the area of each fiber (Fig. 3A a and c), were fitted with Eq. 1. Box plots in Fig. 3B a and

b summarize the distribution of τ_2 of fiber types I, IIA, or IIX. Confirming the observations on live fiber images (Fig. 2B), τ_2 values for type I fibers were statistically significantly separated from those of types IIA and X put together. τ_2 differences between IIA and IIX were not statistically significant (Fig. 3B a and b). Statistical parameters are summarized in Table 1.

The substantial difference in the distributions of τ_2 between types I and II suggested a simple, binary τ_2 threshold criterion as basis for determination of fiber type, according to which fibers with a value <3.3 ns would be assigned as type I, while otherwise fibers would be assigned as type II.

Fluorescence intensity was also tested as an alternative way to identify fiber types. The test is discussed in the Supplemental text. Briefly, we confirmed previous observations of a higher autofluorescence in type I myofibers (Chagnot et al., 2015). However, fluorescence intensity proved fickle, variable in different preparations, and, most problematically, highly susceptible to bleaching. Hence, we abandoned this approach in favor of the use of lifetimes.

Errors of first and second kind in the determination of fiber types

The quality of the proposed method was quantified by estimating its errors of the first and second kind (i.e., probabilities of a false positive or a false negative; Heumann et al., 2016). “Kind” is used instead of the more common denomination “type” to avoid confusion with type as fiber attribute). Let the hypothesis be: “fiber is of type II provided that $\tau_2 > 3.3$ ”; then, the two errors can be estimated as follows, with numbers corresponding to measures in the soleus:

$$\text{Error of the 1st kind} = \frac{\text{\#of type I fibers with } \tau_2 > 3.3 \text{ ns}}{\text{\#of fibers with } \tau_2 > 3.3 \text{ ns}} = \frac{7}{124} = 0.056 \quad (5)$$

and

$$\text{Error of the 2nd kind} = \frac{\text{\#of type II fibers with } \tau_2 \leq 3.3 \text{ ns}}{\text{\#of fibers with } \tau_2 \leq 3.3 \text{ ns}} = \frac{10}{100} = 0.100. \quad (6)$$

Note that an alternative definition of the hypothesis: “fiber is of type I provided that $\tau_2 \leq 3.3$ ” results in a simple exchange of definitions of first and second kind errors, as clarified numerically with Table 2.

A graphical simplification of the method

Having found that the value of the “slow” time constant of the fluorescence response establishes with reasonable certainty the fiber type, we found a practical and fast way to locate myofibers of different types. It uses the “phasor,” or frequency-domain approach to FLIM (Ranjit et al., 2018). The phasor representation combined with available commercial software generates colored masks on optical images, which map ranges of lifetime values, thus producing an initial classification that serves as

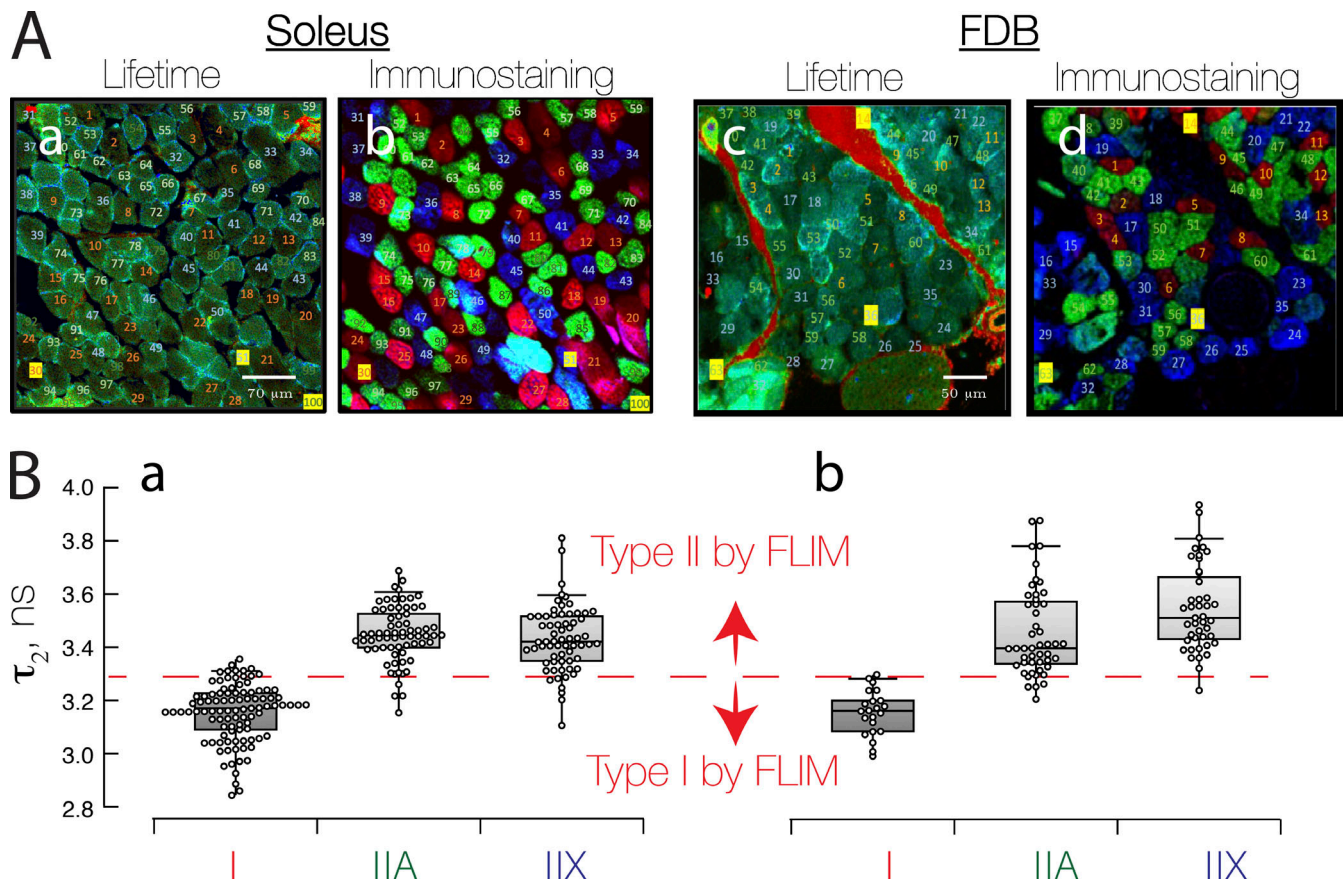


Figure 3. **Correlation of τ_2 maps with immunostaining images in muscle fiber cross-sections.** (A a and c) Autofluorescence lifetime images of soleus and FDB as indicated. (A b and d) Consecutive cryosections immunostained for fiber types I (red), IIA (green), and IIX (blue). (B) Statistics of τ_2 values in fibers identified by immunostaining of cross-sections ($N = 3, m = 231$) for soleus; ($N = 3, m = 113$) for FDB.

guide for further definition of regions where the fluorescence response is characterized analytically with multiexponential fitting. While the approach is fast and practical, it is approximate. An account of its basis and limitations is presented in the Appendix.

An example of this graphic approach is illustrated in Fig. 4. Fig. 4A shows lifetime images; the lifetimes recorded at every pixel were used to construct fluorescence decay curves $I(t)$.

The phasor transform, described in the Appendix, was applied to these time courses to obtain two variables, g and s , that

Table 1. **FLIM parameters found in cross-sections**

	FDB				Soleus			
	τ_1 (ns)	τ_2 (ns)	Te (counts)	m, N	τ_1 (ns)	τ_2 (ns)	Te (counts)	m, N
Type I	0.49	3.16	317	22, 3	0.46	3.16	372.1	97, 3
S.E.M	0.007	0.03	29		0.004	0.01	17.1	
p for types I vs. IIA	<0.001**	<0.001**	<0.001**		<0.001**	<0.001**	0.02*	
Type IIA	0.67	3.46	143	48, 3	0.58	3.44	307.2	69, 3
SEM	0.008	0.03	32.6		0.003	0.01	22.2	
p for types I vs. IIX	<0.001**	<0.001**	<0.001**		<0.001**	<0.001**	0.07	
Type IIX	0.65	3.55	221	43, 3	0.56	3.46	436	65, 3
SEM	0.01	0.02	15		0.004	0.01	30.6	
p for types IIA vs. IIX	0.53	0.01*	<0.001**		0.002*	0.81	0.002*	

Quantitative outcomes of the analysis of FLIM data, defined in Materials and methods. The p 's are probabilities of no difference in the comparison listed, calculated by nested analysis. Asterisks mark changes statistically significant at the <0.05 (*) and <0.001 (**) level.

Table 2. Errors in the acceptance or rejection when recognizing a fiber type

	# type I fiber w/ $\tau_2 > 3.3$	All fibers w/ $\tau_2 > 3.3$	First kind error	# type II fiber w/ $\tau_2 < 3.3$	All fibers w/ $\tau_2 < 3.3$	Second kind error	N, m
FDB ^a	1	85	0.01	6	27	0.22	3, 113
Soleus ^a	7	124	0.056	10	100	0.1	3, 231
	# type II fiber w/ $\tau_2 < 3.3$	All fibers w/ $\tau_2 < 3.3$	First kind error	# type I fiber w/ $\tau_2 > 3.3$	All fibers w/ $\tau_2 > 3.3$	Second kind error	N, m
FDB ^b	6	27	0.22	1	85	0.01	3, 113
Soleus ^b	10	100	0.1	7	124	0.056	3, 231

^aWhen recognizing a fiber as type I.

^bWhen recognizing a fiber as type II.

represent every pixel by a vector (phasor) in phasor space (Fig. 4B c and d, where color corresponds to the number of pixels with phasor in the same range).

Note that the phasors cluster near two values. The software allows the reverse mapping, from regions within circles in phasor space to the corresponding pixels in “lifetime space” (Fig. 4B a and b), forming masks that overlap approximately with individual myofibers. While fluorescence decays with different time courses may have similar phasors (as shown in the

Appendix), we have found in the present study a good correspondence between phasor location and τ_2 value. This empirical observation is evident in the clear distinction of myofibers corresponding to the two most intense clusters in both phasor images (Fig. 4B c and d).

The autofluorescence originates in FAD

As a step toward understanding the chemical basis of this empirical method and eventually using lifetimes as monitors of metabolic properties, we compared spectra of fluorescence emission of live muscle fibers and FAD containing solutions, a study illustrated with Fig. 5.

We found that these FAD spectra, with maxima at ~ 525 nm, overlapped closely with the corresponding spectra of autofluorescence, which largely confirms prior observations (e.g., Huang et al., 2002) that largely attribute autofluorescence to FAD. Note, however, the separation at both extremes of the abscissa, which suggests the presence of multiple fluorescent species (e.g., riboflavin and FMN; Surre et al., 2018). $I(t)$ was also acquired at multiple free flavin concentrations between 10 μ M and 20 mM (as shown in Fig. 5B, inset).

Discussion

The method described here aims to identify the type of a myofiber by the value of one of the exponential decay time constants of the autofluorescence response to a brief excitation. To establish the method, paired cryosections were compared by measuring the photon arrival time (lifetime) in the first section,

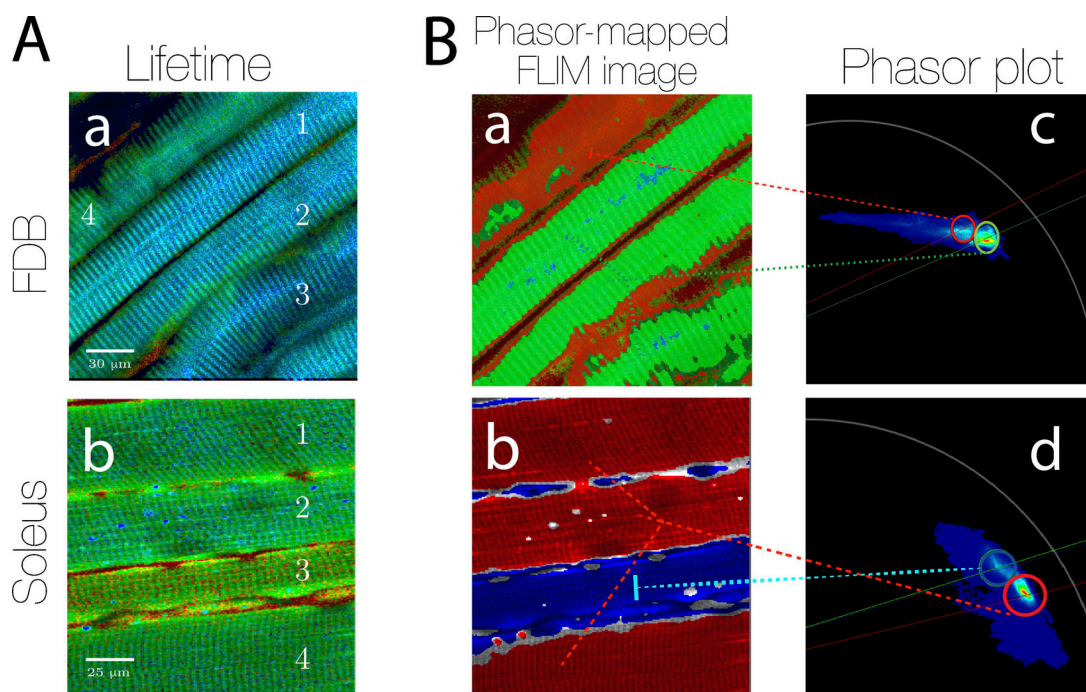


Figure 4. Identification of fiber types in longitudinal sections of live muscles. (A a and b) Lifetime images of autofluorescence in FDB and soleus. (B a and b) Phasor maps, which display the approximate regions within fibers corresponding to a particular τ value. (B c and d) Phasor plots, resulting from application of the phasor transform (described in the Appendix) to the lifetime data in A; higher values of the abscissa correspond to lower arrival times, hence lower τ_2 . The maps in B a and b are created by selecting the regions of high signal in the phasor plots.

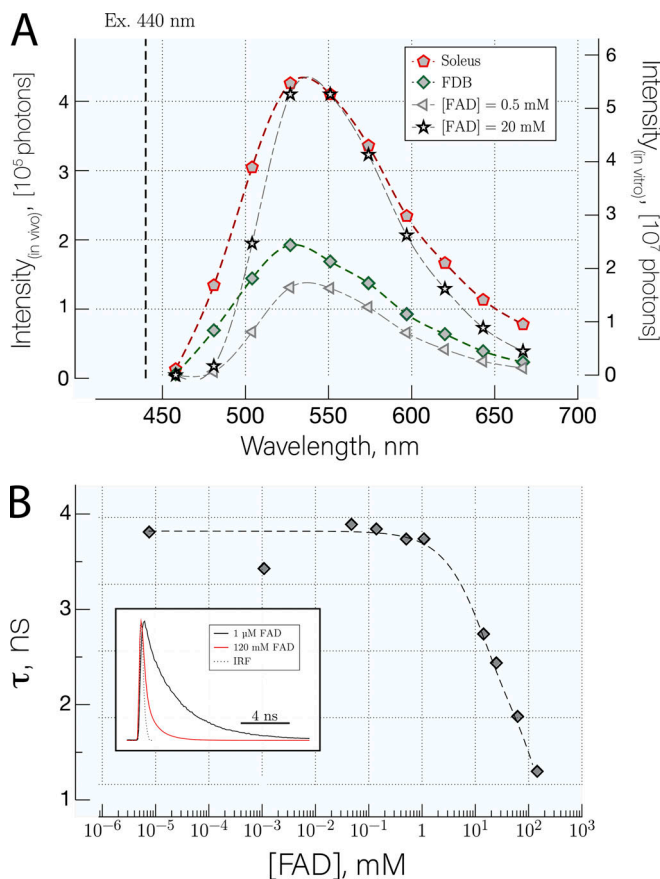


Figure 5. **Fluorescence properties of FAD in solution compared with muscle autofluorescence.** (A) Emission spectrum of FAD; excitation was set at 440 nm. Measurements were performed in vivo in soleus and FDB muscles, and in vitro with two solutions of different free FAD concentrations. (B) In vitro measurements of τ at increasing [FAD]. The arrival time histograms or fluorescence responses $I(t)$ obtained at the extremes of the FAD concentration range are shown in the inset. They are well fitted by single exponentials of time constant τ .

and immunostaining of MHC in the next one. On this basis, we defined a simple binary criterion that separates types I and II based on a threshold value, 3.3 ns, of the cell-averaged τ_2 , in the two-exponential fit that the autofluorescence transients almost always satisfy.

Given the major differences in protein endowment and function between fiber types, fiber “typing” has been a long-sought goal when interpreting functional and structural measurements. This is sometimes achieved by immunological techniques or simply by sourcing myofibers from muscles in which one type predominates. The approach we propose here has obvious advantages over the prior approaches: it applies to live tissue, is noninvasive as it requires neither exogenous monitors nor high-intensity illumination, is fast, and can be implemented in a practical graphic manner by transitioning between the time and frequency (phasor) domains (as illustrated with Fig. 4).

The major limitation of the novel technique is that it is approximate, subject to errors for which we provided estimates. The asymmetries in these errors are worth noting. Thus, a

classification of a fiber as type II, based on a $\tau_2 > 3.3$ ns, will be in error 1% of the time; the converse, a diagnosis of type I on the basis of a $\tau_2 < 3.3$ ns, will be in error in approximately one of every five cases (see Table 2 for clarification). These errors can be reduced by making the criterion more stringent; for example, lowering the threshold, in soleus muscle, for a positive classification of type I (e.g., to 3.2 ns), would reduce the error to 2/57 (number of type II fibers with $\tau_2 < 3.2$ ns / all fibers with $\tau_2 < 3.2$ ns) = 0.03. An increase in the threshold τ_2 value used to identify type II fibers would correspondingly reduce errors in their identification. These more stringent definitions would, of course, leave some fibers in an “undetermined type” category.

Here, we showed that the emission spectrum of FAD in solution is similar, albeit not identical, to that of the autofluorescence observed in both soleus and FDB, which is consistent with the dominant role attributed to flavins as sources of the autofluorescence excited by visible light in muscle (e.g., Surre et al., 2018). Myofibers have characteristic concentrations of free and protein-bound flavins, which depend on fiber type and activity. We show here a correspondence between fiber type and autofluorescence lifetimes, while also demonstrating a negative correlation between lifetime and FAD concentration in solutions. Jointly, the observations suggest a tentative explanation for the difference in τ_2 of the autofluorescence: oxidized FAD levels are higher in type I than in IIA or IIX (Chemello et al., 2011; Chagnot et al., 2015). In addition to differences in protein bound versus free states of flavins, these results point at differences in redox states as causes for the observed divergence of lifetimes. Because the present measurements were performed in young and healthy animals, it will be necessary to again characterize lifetimes when applying the procedure to a different animal model, pathophysiological condition, or muscle.

Fluorescence intensity has been the commonly used variable when measuring autofluorescence of intracellular metabolites (for a review, see Kolenc and Quinn, 2019). Using this variable as an alternative way to determine the types of fibers in a muscle was tested in this work (see Fig. S1). Intensity-based measurements of FAD/FMN bring some advantages, such as a better signal-to-noise ratio than lifetime measurements. However, it brings more limitations, as this intensive variable depends on parameters used to collect data and, therefore, is inconsistent in assigning a quantitative value to each fiber type. In our study, illustrated in the Supplemental text, photobleaching proved the most conspicuous (see Fig. S2) source of variability in intensity—a consequence of both the susceptibility of FAD and related molecules to bleaching and their low concentrations, requiring high-excitation intensity. A different intrinsic fluorophore, such as NADH, would be superior, as it is found at higher concentrations than FAD. Its use, however, is limited by the requirement for excitation in the deep UV.

In conclusion, we demonstrated the potential value of FLIM to discriminate between fiber types I and II in two muscles with dissimilar proportions of oxidative and glycolytic fibers. This simple, fast, and non-invasive method should help standardize functional assays for which results are expected to depend on myofiber type.

Appendix: Phasor analysis as graphic shortcut to identification of fiber type

The appendix provides a summary description of the phasor analysis of FLIM data, followed by a discussion of the basis and limitations of its use for the purposes of myofiber typing.

The phasor plot

For lifetime measurements, excitation light is pulsed at a constant frequency. The excitation profile can, therefore, be represented by a discrete spectrum of sinusoidal functions of time, of frequencies that are multiples of the fundamental. The emission response is equally decomposable into sinusoidal signals. The response of a single molecular species to each sinusoidal term will be the product of each term by a constant phase vector or phasor, defined by two numbers: amplitude (m) and phase (θ), or two projections, $g (= m \cos \theta)$ and $s (= m \sin \theta)$, on orthogonal coordinate axes, which define a point in 2-D phasor space (Ranjit et al., 2018; Digman et al., 2008). A simple formula links the two components in phasor space to a time-dependent decay $I(t)$:

$$g(w) = \frac{\int_0^\infty I(t) \cos(wt) dt}{\int_0^\infty I(t) dt} \quad s(w) = \frac{\int_0^\infty I(t) \sin(wt) dt}{\int_0^\infty I(t) dt}, \quad (7)$$

where w is the fundamental angular frequency of excitation, i.e., $w = 2\pi/\text{pulse interval}$. In other words, the phasor is the complex weight of the Fourier transform of the temporal decay of fluorescence at the pulsing frequency.

Fourier decomposition has the computational advantage of removing the time dependence of signals, and leaving just a constant vector for every component in multicomponent responses. Applied to fluorescent systems with few molecular species, as in the present case, it produces a representation of the system that conveys its fluorescence lifetime properties

graphically, in the phasor plot, whereby every pixel in the FLIM image is represented by a point at the tip of its phasor (Fig. A1). If the decay is a single exponential, $I(t) = Ae^{-t/\tau}$, the phasor coordinates are

$$g(w) = \frac{1}{1 + w^2\tau^2} \quad s(w) = \frac{w\tau}{1 + w^2\tau^2}; \quad (8)$$

therefore, the tip of the phasor describes a semicircle (known as the universal circle; e.g., Digman et al., 2008). In this semicircle, longer lifetimes tend to be displayed to the left and shorter ones to the right.

When the time response can be fitted as the sum of two decaying exponentials (Eq. 1), the corresponding phasors will occupy points—or clusters, allowing for noise—along the segment in phasor space that connects the two points on the circle, p_1 and p_2 , corresponding to τ_1 and τ_2 via Eq. 8 (Fig. A1). Phasor locations in this segment can also correspond to other systems with multiexponential decays, including a biexponential with time constants different than τ_1 and τ_2 , as illustrated in the figure.

LASX, the analysis software provided by the instrument supplier (Leica) for time-domain photon counting and frequency-domain (phasor) FLIM allows mapping between the two representational spaces, so that selecting a region of the phasor plot that represents a particular combination of time constants and amplitudes results in the highlight of corresponding areas of the phasor-mapped FLIM image (Fig. A1; and Fig. 4B a and b), for immediate identification of myofibers with different properties. This method provides rapid and qualitative visualization of groups of cells and helps identify groups of fibers with characteristic fluorescence lifetimes.

Errors of the method estimated from the comparison between images in muscle fiber cross-sections. If the single lifetime threshold criterion is used, the classification is binary (fibers are classified as either type I or type II) and the two kinds

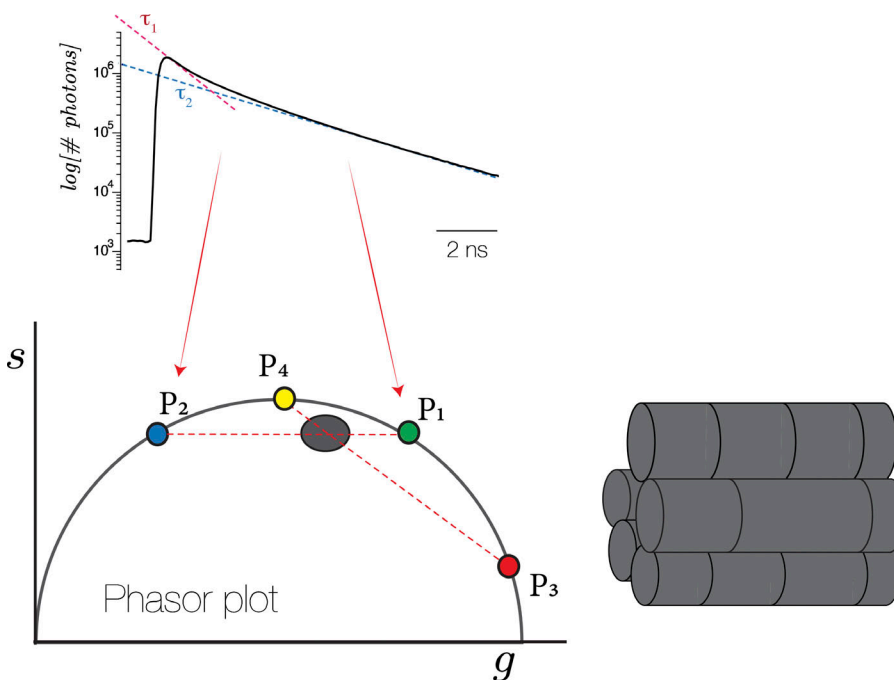


Figure A1. **Frequency-domain analysis maps pixel fluorescence times to points in phasor space.** A Fourier transformation maps the fluorescence decay (or histogram of photon arrival times) illustrated in the legend of Fig. 1E to points in phasor space of coordinates g and s given by Eq. 7. Single-exponential fluorescence decays map to points on the “universal circle” (actually, a semicircle, where points of greater g value correspond to shorter time constants). Multiexponential decays map to points inside the circle. A two-component decay with lifetimes τ_1 and τ_2 will map to a point in the segment joining the single-exponential points (p_1 and p_2) on the universal circle. Multiple combinations of two (or more) exponential decays of different time constants may map to the same point in phasor space, for example, at the intersection of the segments p_1 - p_2 and p_3 - p_4 , which corresponds to the two-exponential decay with constants τ_3 and τ_4 .

of error trade places when identifying one type or the other. More stringent criteria involving two threshold lifetimes, th_1 , the top lifetime for type I myofibers, and th_2 , the minimum lifetime for type II, will reduce errors and leave fibers, those with lifetimes between th_1 and th_2 , without typing.

Acknowledgments

Olaf S. Andersen served as editor.

This paper was supported by the following grants from the National Institute of Arthritis and Musculoskeletal and Skin, National Institutes of Health, USA: AR072602 to S.L. Hamilton, F. Horrigan, S.Y. Jung, and E. Rios, and AR068312 to E. Rios, M. Fill, and S. Riazi.

The authors declare no competing financial interests.

Author contributions: Conceptualization: C. Manno, L. Figueroa. Data curation: C. Manno, E. Tamminen, L. Figueroa. Formal analysis: C. Manno. Methodology: C. Manno, E. Tamminen. Resources: E. Rios. Validation: C. Manno, Y. Oropeza-Almazan, E. Rios. Visualization: C. Manno, L. Figueroa. Writing (original draft): C. Manno. Writing (review & editing): C. Manno, L. Figueroa, E. Rios.

Submitted: 1 March 2022

Accepted: 13 June 2022

References

- Baylor, S.M., and S. Hollingworth. 2003. Sarcoplasmic reticulum calcium release compared in slow-twitch and fast-twitch fibres of mouse muscle. *The Journal of physiology*. 551:125–138. <https://doi.org/10.1113/jphysiol.2003.041608>
- Beedle, A.M.. 2016. Cryosectioning of contiguous regions of a single mouse skeletal muscle for gene expression and histological analyses. *JoVE*. <https://doi.org/10.3791/55058>
- Blinova, K., S. Carroll, S. Bose, A.V. Smirnov, J.J. Harvey, J.R. Knutson, and R.S. Balaban. 2005. Distribution of mitochondrial NADH fluorescence lifetimes: Steady-state kinetics of matrix NADH interactions. *Biochemistry*. 44:2585–2594. <https://doi.org/10.1021/bi0485124>
- Calderon-Velez, J.C., P. Bolaños, and C. Caputo. 2010. Myosin heavy chain isoform composition and Ca^{2+} transients in fibres from enzymatically dissociated murine soleus and extensor digitorum longus muscles. *J. Physiol.* 588:267–279. <https://doi.org/10.1113/jphysiol.2009.180893>
- Chagnot, C., A. Vénien, F. Peyrin, F. Jamme, M. Réfrégiers, M. Desvaux, and T. Astruc. 2015. Deep UV excited muscle cell autofluorescence varies with the fibre type. *The Analyst*. 140:4189–4196. <https://doi.org/10.1039/c5an00172b>
- Chemello, F., C. Bean, P. Cancellara, P. Laveder, C. Reggiani, and G. Lanfranchi. 2011. Microgenomic analysis in skeletal muscle: Expression signatures of individual fast and slow myofibers. *PLoS One*. 6:e16807. <https://doi.org/10.1371/journal.pone.0016807>
- Chen, L.-C., W.R. Lloyd, S. Kuo, H.M. Kim, C.L. Marcelo, S.E. Feinberg, and M.-A. Mycek. 2014. The potential of label-free nonlinear optical molecular microscopy to non-invasively characterize the viability of engineered human tissue constructs. *Biomaterials*. 35:6667–6676. <https://doi.org/10.1016/j.biomaterials.2014.04.080>
- Digman, M.A., V.R. Caiolfa, M. Zamai, and E. Gratton. 2008. The phasor approach to fluorescence lifetime imaging analysis. *Biophysical journal*. 94:L14–L16. <https://doi.org/10.1529/biophysj.107.120154>
- Heumann, C., M. Schomaker, and Shalabh. 2016. Introduction to statistics and data analysis, with exercises, solutions and applications in R. Springer. <https://doi.org/10.1007/978-3-319-46162-5>
- Hollingworth, S., and M.W. Marshall. 1981. A comparative study of charge movement in rat and frog skeletal muscle fibres. *J. Physiol.* 321:583–602. <https://doi.org/10.1113/jphysiol.1981.sp014004>
- Huang, S., A.A. Heikal, and W.W. Webb. 2002. Two-photon fluorescence spectroscopy and microscopy of NAD(P)H and flavoprotein. *Biophysical journal*. 82:2811–2825. [https://doi.org/10.1016/s0006-3495\(02\)75621-x](https://doi.org/10.1016/s0006-3495(02)75621-x)
- Johnson, D.T., R.A. Harris, P.V. Blair, and R.S. Balaban. 2007. Functional consequences of mitochondrial proteome heterogeneity. *American journal of physiology. Cell physiology*. 292:C698–C707. <https://doi.org/10.1152/ajpcell.00109.2006>
- Kolenc, O.I., and K.P. Quinn. 2019. Evaluating cell metabolism through autofluorescence imaging of NAD(P)H and FAD. *Antioxid. Redox Signaling*. 30:875–889. <https://doi.org/10.1089/ars.2017.7451>
- Lakowicz, J. 2006. Principles of Fluorescence Spectroscopy. Third edition. Vol. 287. Springer.
- Lakowicz, J.R., H. Szmacinski, K. Nowaczyk, and M.L. Johnson. 1992. Fluorescence lifetime imaging of free and protein-bound NADH. *Proceedings of the National Academy of Sciences of the United States of America*. 89:1271–1275. <https://doi.org/10.1073/pnas.89.4.1271>
- Lazic, S.E., C.J. Clarke-Williams, and M.R. Munafò. 2018. What exactly is “N” in cell culture and animal experiments? *PLoS biology*. 16:e2005282. <https://doi.org/10.1371/journal.pbio.2005282>
- Manno, C., L.C. Figueroa, D. Gillespie, R. Fitts, C. Kang, C. Franzini-Armstrong, and E. Rios. 2017. Calsequestrin depolymerizes when calcium is depleted in the sarcoplasmic reticulum of working muscle. *Proc. Natl. Acad. Sci. USA*. 114:E638–E647. <https://doi.org/10.1073/pnas.1620265114>
- Periasamy, A., and R. Clegg. 2009. FLIM Microscopy in Biology and Medicine. Chapman and Hall. 474.
- Ranjit, S., L. Malacrida, D.M. Jameson, and E. Gratton. 2018. Fit-free analysis of fluorescence lifetime imaging data using the phasor approach. *Nature protocols*. 13:1979. <https://doi.org/10.1038/s41596-018-0026-5>
- Schiaffino, S., L. Gorza, S. Sartore, L. Saggin, S. Ausoni, M. Vianello, K. Gundersen, and T. Lømo. 1989. Three myosin heavy chain isoforms in type 2 skeletal muscle fibres. *Journal of muscle research and cell motility*. 10:197–205. <https://doi.org/10.1007/bf01739810>
- Sikkel, M.B., D.P. Francis, J. Howard, F. Gordon, C. Rowlands, N.S. Peters, A.R. Lyon, S.E. Harding, and K.T. MacLeod. 2017. Hierarchical statistical techniques are necessary to draw reliable conclusions from analysis of isolated cardiomyocyte studies. *Cardiovascular research*. 113:1743–1752. <https://doi.org/10.1093/cvr/cvx151>
- Surre, J., C. Saint-Ruf, V. Collin, S. Orenge, M. Ramjeet, and I. Matic. 2018. Strong increase in the autofluorescence of cells signals struggle for survival. *Scientific reports*. 8:12088. <https://doi.org/10.1038/s41598-018-30623-2>

Supplemental material

Fluorescence lifetime of autofluorescence, a novel method to determine murine skeletal muscle fiber types

This supplement demonstrates that intensity of autofluorescence could be useful for myofiber typing, but has significant disadvantages compared with the evaluation of fluorescence lifetimes.

Fig. S1A a, b, and c illustrate τ_2 maps of serial cryosections, autofluorescence intensities determined together, and corresponding immunostaining of type I and IIA fibers, respectively (as described in the FLIM of autofluorescence section of Materials and methods). After immunostaining, an identification number was assigned to fibers chosen randomly, to subsequently compare with corresponding lifetime values determined in the next cross-section. Lifetime and intensity values determined for type-identified fibers were cross-plotted as illustrated in Fig. S1A c. Fluorescence intensity was highly negatively correlated with lifetime values.

Using a freshly isolated soleus muscle imaged longitudinally, fluorescence intensity was measured in regions of interest covering the area of a myofiber. τ_1 , τ_2 , and fluorescence intensity are plotted as a function of time in Fig. S2. Lifetime signals are constant over the 45-s acquisition period, but the fluorescence intensity decays, reflecting rapid bleaching under the excitation needed to reveal the autofluorescence. While the intensity measured in the cross-sections is systematically higher for type II fibers, consistent with its use for type identification, the rapid bleaching constitutes a major limitation, contrasting with the robust measure of lifetimes over the same period.

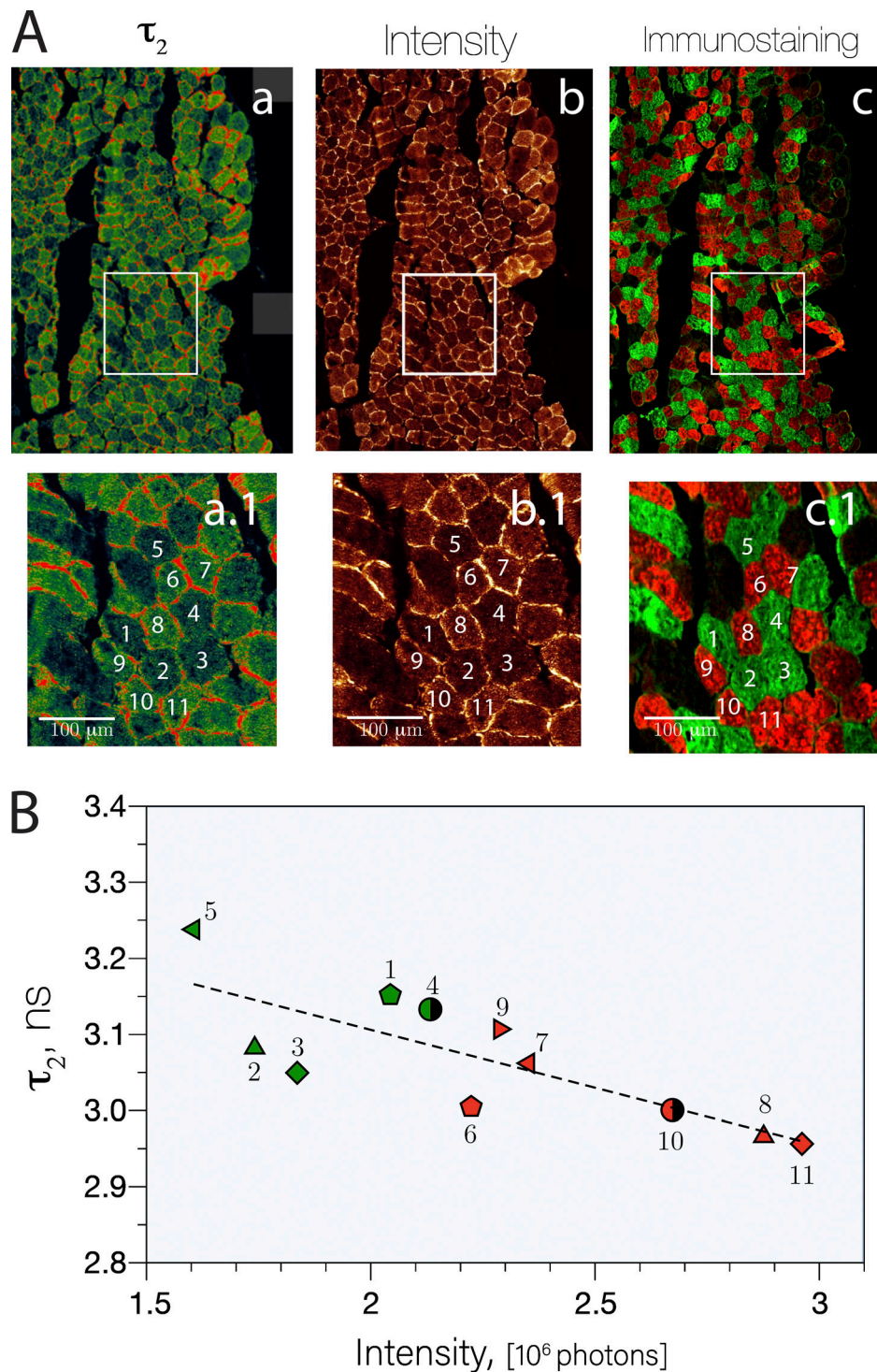


Figure S1. **Identification of fiber types with immunostaining and FLIM images in soleus muscle cross-sections.** (A) For a wider view of the sample, arrays of several 256×256 -pixel images were scanned and merged together to form. (A a) Autofluorescence lifetime color map. (A b) FAD fluorescence intensity image. (A c) Immunostaining identifying fiber types I (red) and IIA (green) in a consecutive cryosection. Amplified regions of the whole muscle cross-section, delimited by white frames, are displayed in insets a.1–c.1. After immunostaining, an identification number was assigned to fibers chosen randomly, 1–5 for type IIA (green) and 6–11 for type I (red), to subsequently match up with fibers acquired with FLIM in the next cross-section. (B) Immunostained fibers were assigned a lifetime and intensity value, which showed that type I fibers (red symbols) correlated with high intensity and low τ_2 , and type IIA fibers (green symbols) with low intensity and higher lifetime.

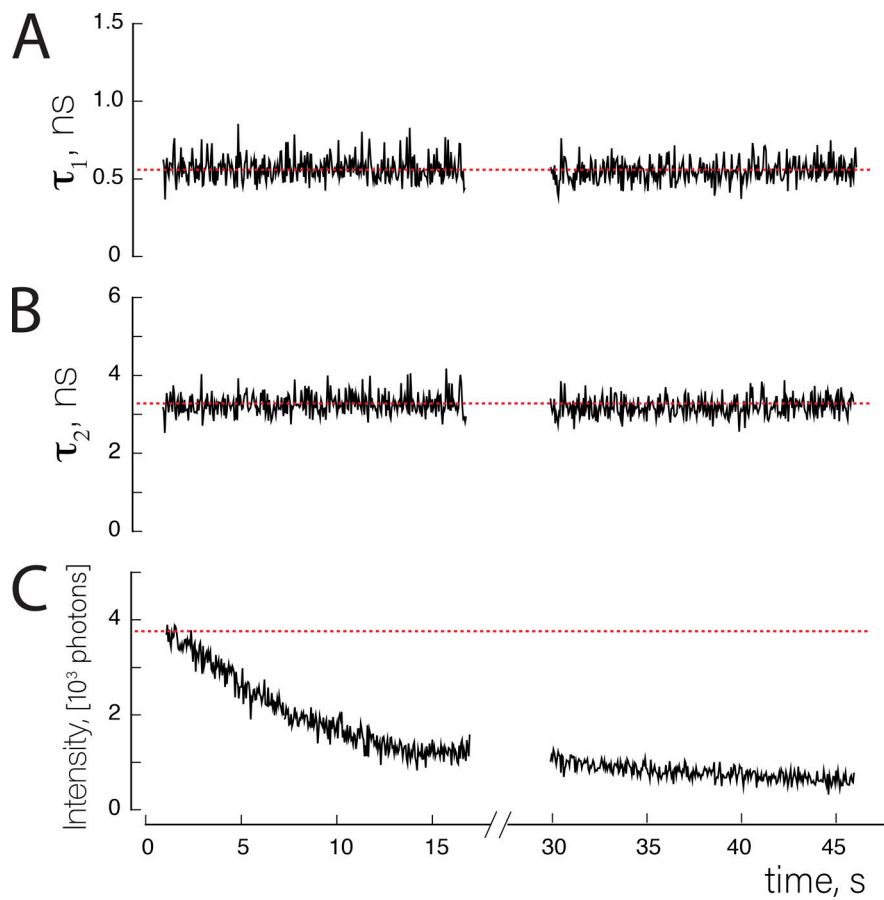


Figure S2. **FLIM parameters measured in xt-linescan mode.** Lifetimes 1 and 2 (A and B, respectively) remained constant when pulses of excitation at 440 nm were constantly applied for 15 s. **(C)** The intensity of fluorescence, on the other hand, steadily decayed as it was bleached during this period of illumination.